

Shear flows and their suppression at large aspect ratio. Two-dimensional simulations of a growing convection zone

J. R. Fuentes and A. Cumming

*Department of Physics and McGill Space Institute, McGill University,
3600 rue University, Montreal, QC H3A 2T8, Canada*

We investigate the onset and evolution of zonal flows in a growing convective layer when a stably-stratified fluid with a composition gradient is cooled from above. This configuration allows the study of zonal flows for a wide range of values of the Rayleigh number, Ra , and aspect ratio of the convection zone within a given simulation. We perform a series of 2D simulations using the Boussinesq approximation, with aspect ratio of the computational domain between 1 and 5, and Prandtl number $Pr = 0.1, 0.5, 1$, and 7. We find that for square domains zonal flows appear when the aspect ratio of the convective layer is smaller than two, and the evolution of the system depends on the Prandtl number. For $Pr \leq 1$, the fluid experiences bursts of convective transport with negligible convective transport between bursts. The magnitude and frequency of the bursts are smaller at low Pr , which suggests that the bursting regime is stronger in a narrow range around $Pr = 1$, as observed in previous studies of thermal convection. For $Pr = 7$, the structure of the flow consists of tilted convective plumes, and the convective transport is sustained at all times. In wider domains, the aspect ratio of the convective zone is always much larger than two and zonal flows do not appear. These results confirm and extend to fluids with stable composition gradients previous findings on thermal convection. The fact that zonal flows can be avoided by using computational domains with large aspect ratios opens up the possibility of 2D studies of convective overshoot, layer formation and transport properties across diffusive interfaces.

I. INTRODUCTION

Large scale horizontal flows (hereafter) arise in many geophysical and astrophysical fluids, particularly in convective systems where the fluid motions are approximately two-dimensional, such as rotating flows in planetary atmospheres, where the Taylor-Proudman effect suppresses fluid motions parallel to the axis of rotation [1, 2]. These flows are of great interest because of their chaotic non-linear behavior and also because of the effects they have on mixing and transport properties.

Thermal convection in two-dimensions at large Rayleigh number (Ra^1) has been used extensively as the canonical model to study zonal flows in convection. A remarkable result from previous studies of zonal flows is that the nature of the fluid and the transport properties depend strongly on the Prandtl number (Pr^1) [3–6]. In particular, it has been shown that once the convective flow is affected by large-scale horizontal motions at large Ra , for low Pr ($\lesssim 1$) it undergoes strong oscillations and heat transport occurs in chaotic bursts, whereas for higher Pr the flow does not burst and vertically-sheared thermal plumes dominate the structure of the flow at all times. In both regimes, once the zonal flow sets in, its net effect is the decrease of the vertical heat transport. Interestingly, bursts and sheared convective plumes have also been found in two-dimensional simulations of fingering convection [e.g., 7–9], and as with zonal flows in thermal convection, they decrease the vertical transport of heat and solute.

Thompson [10] suggested that zonal flows in two-dimensional convection are sustained against viscous diffusion by Reynold stresses. By perturbing convective cells with a small shear flow, the shear advects convective plumes, tilting

them with respect to the vertical. The Reynolds stresses associated with the tilted plumes transport momentum across the vertical, enhancing the shear flow and therefore the amplitude of the shear perturbations. This mechanism is called tilting instability and energy is supplied directly from the convective scales to the zonal flow. Although a different mechanism has been proposed to explain the zonal flow [see, e.g., 11, who proposed that zonal flow generation can be due to an energy transfer from small to large scale motions], the tilting mechanism has been shown to be operating in numerical simulations and theoretical models [3, 12].

Zonal flows have also been observed in old laboratory experiments of Rayleigh-Benard convection in water confined to a horizontal layer [13, 14]. However, the properties and the different regimes described above have not been observed in later experiments nor in three-dimensional numerical simulations [15, 16], unless an external mechanism induces them [17, 18]. Furthermore, Hartlep *et al.* [15] demonstrated that convective rolls of large horizontal extent can arise at large Ra in three-dimensional simulations, and suggested them as a better interpretation of the observations, rather than the zonal flows that appear in two-dimensional convection.

Besides the importance of characterizing the morphology and transport properties of zonal flows in convection, the effects discussed above raised the question of whether two-dimensional simulations are appropriate to study convection problems in general. Since three-dimensional simulations are computationally expensive, two-dimensional simulations are often adopted to study convection in different systems. By comparing the outcomes of 2D and 3D simulations of fingering convection at low Pr , Garaud and Brummell [7] pointed out that 2D simulations are not appropriate since the shear effects of artificial zonal flows significantly decrease the vertical transport, and change the structure and morphology of the flow. However, recent work by Fitzgerald and Farrell [5] and Wang *et al.* [19] have shown that for the case of pure thermal

¹See Sect. II for a definition.

convection, zonal flows are not sustained in two-dimensional simulations using domains of large aspect ratio.

Whether zonal flows appear in fluids with stable composition gradients has not been explored yet. If they do, it is not clear if they can be suppressed at large aspect ratio as for the case of thermal convection. The answers to these questions are important for example for two-dimensional studies of turbulent mixing and layer formation in double-diffusive convection.

In this work, we report two-dimensional simulations of convection driven by a constant heat flux at the top boundary in a stable fluid with a solute gradient. This configuration is particularly useful to study the onset and evolution of zonal flows. The solute gradient stabilizes the fluid against overturning convection in the whole fluid domain, leaving a convective layer whose thickness increases with time. The aspect ratio of the convective layer in a given simulation decreases in time as the thickness of the layer grows. This allows the study of convection for a wide range of Ra and aspect ratio using a smaller grid of simulations. Further, it provides an opportunity to study the transition to sheared convection once the zonal flow arises. We perform simulations at Pr ranging from 0.1 to 7 in order to explore the bursting and non-bursting regimes. We also perform simulations with fluid domains of different aspect ratio to confirm that zonal flows and their shear effects do not appear at large aspect ratio, as observed in previous studies of thermal convection.

The paper is organised as follows. Sect. II presents the model and the numerical code used to perform the simulations. In Sect. III A we study the onset of zonal flows and the bursting and non-bursting regimes in simulations with aspect ratio of one, i.e., square domains ($L = H$). In Sect. III B we show that strong horizontal flows and their effects vanish when the width of the domain is increased ($L \geq 2H$). We conclude in Sect. IV.

II. MODEL AND NUMERICAL METHOD

We study the onset and evolution of zonal flows in a two-dimensional convective layer that grows inward by incorporating fluid from below. These simulations are based on our previous study [20] that was focused on the rate at which the convection zone grows inwards. However, in the previous work we deliberately excluded those simulations that developed shearing convection. In the simulations, we model the fluid under the Boussinesq approximation [21], which is appropriate when the density variations are small respect to the background density ($\rho/\rho_0 \ll 1$). The fluid domain is a Cartesian box in two-dimensions (x, z) of width L and height H , with periodic boundary conditions in the horizontal direction. The top and bottom boundaries are impermeable and stress-free, with no composition flux through them, no heat flux at the bottom, and a constant heat flux F_0 at the top. Initially, the fluid starts with a uniform temperature and a constant solute gradient $dS_0/dz = -\delta S_0/H < 0$, such that the solute concentration is two times larger at the bottom compared to the top. The evolution of the system is driven by the imposed heat flux

F_0 at the top boundary, which cools the fluid from the top and quickly forms a convective layer that grows inwards.

As we mentioned above, this numerical set-up is ideal to study the onset of the zonal flow in the simulations. First, two dimensionality prevents transverse perturbations that can reduce horizontal fluid motions. Second, periodic boundary conditions on the side boundaries do not confine the fluid in the horizontal direction. Third, the free-slip top and bottom boundaries apply no shear stresses to slow down the horizontal flow. Further, since the onset of the zonal flow depends on the aspect ratio of the convective layer, the time-dependent nature of the convective layer thickness is ideal to study the critical aspect ratio at which the zonal flow arises.

Following Sect. 2 in [20], we non-dimensionalize the variables using as characteristic length and time scales the box height, H , and the thermal diffusion time across the box, H^2/κ_T (where κ_T is the thermal diffusivity). Solute concentration is measured in units of the initial solute contrast across the box, δS_0 , and temperature is in units of the initial solute contrast, $\beta\delta S_0/\alpha$ (here β and α are the coefficients of solute and thermal contraction-expansion, respectively). The resulting dimensionless equations are

$$\nabla \cdot \mathbf{v} = 0, \quad (1)$$

$$\frac{\partial T}{\partial t} = -(\mathbf{v} \cdot \nabla) T + \nabla^2 T, \quad (2)$$

$$\frac{\partial S}{\partial t} = -(\mathbf{v} \cdot \nabla) S + \tau \nabla^2 S, \quad (3)$$

$$\frac{\partial \mathbf{v}}{\partial t} = -(\mathbf{v} \cdot \nabla) \mathbf{v} - \nabla P + \mathcal{R}_T Pr \left(\frac{F_0}{F_{\text{crit}}} \right)^{-1} \hat{\mathbf{z}} + Pr \nabla^2 \mathbf{v}, \quad (4)$$

with boundary conditions

$$w|_{z=0,1} = 0, \quad \frac{\partial u}{\partial z}|_{z=0,1} = 0, \quad \frac{\partial S}{\partial z}|_{z=0,1} = 0, \quad (5)$$

$$\frac{\partial T}{\partial z}|_{z=0} = 0, \quad \frac{\partial T}{\partial z}|_{z=1} = -\frac{F_0}{F_{\text{crit}}}. \quad (6)$$

The dimensionless parameters that control the simulations are F_0/F_{crit} , the Prandtl number (Pr), the diffusivity ratio (τ) and a modified Rayleigh number (\mathcal{R}_T), defined respectively as

$$\frac{F_0}{F_{\text{crit}}} = F_0 \left(k \frac{\beta}{\alpha} \frac{\delta S_0}{H} \right)^{-1}, \quad (7)$$

$$Pr = \frac{\nu}{\kappa_T}, \quad (8)$$

$$\tau = \frac{\kappa_S}{\kappa_T}, \quad (9)$$

$$\mathcal{R}_T = \frac{\alpha g H^3}{\kappa_T \nu} \left(\frac{F_0 H}{k} \right), \quad (10)$$

where k is the thermal conductivity, ν , and κ_S are the viscous and solute diffusivity, respectively, and g is the magnitude of the acceleration due to gravity. As we note in [20], the product

TABLE I. Dimensionless parameters used in the simulations. The first and second columns correspond to the diffusivity ratio and Prandtl number, respectively. The third column contains the input cooling flux at the top boundary, and the last two columns contain the modified Rayleigh numbers for temperature and solute, respectively.

#	τ	Pr	F_0/F_{crit}	\mathcal{R}_T	\mathcal{R}_S
1	0.1	0.1	5.4	4×10^{12}	7.5×10^{11}
2	0.1	0.1	10.8	8×10^{12}	7.5×10^{11}
3	0.1	0.5	5.4	8×10^{11}	1.5×10^{11}
4	0.1	0.5	10.8	1.6×10^{12}	1.5×10^{11}
5	0.1	1	5.4	4×10^{11}	7.5×10^{10}
6	0.1	1	10.8	8×10^{11}	7.5×10^{10}
7	0.1	7	5.4	5.76×10^{10}	1.06×10^{10}
8	0.1	7	10.8	1.15×10^{11}	1.06×10^{10}

$\mathcal{R}_T(F_0/F_{\text{crit}})^{-1}$ can be re-written as

$$\mathcal{R}_T \left(\frac{F_0}{F_{\text{crit}}} \right)^{-1} = \mathcal{R}_S = \frac{\beta g H^3 \delta S_0}{\kappa_T \nu}, \quad (11)$$

which resembles the traditional Rayleigh-number

$$Ra = \frac{\alpha g H^3 \delta T_0}{\kappa_T \nu}, \quad (12)$$

but for solute. The parameters used in our simulations are given in Table I.

The governing differential equations are solved with the Dedalus spectral code [22] on a Chebyshev (vertical) and Fourier (horizontally-periodic) domain in which the physical grid dimensions are 3/2 the number of modes. Based on a resolution study, we use 1024 modes in each direction.

III. ANALYSIS AND RESULTS

A. Zonal flow and sheared convection in square domains

As soon as the heat flux at the top boundary turns on, a thermal boundary layer develops and becomes convective. The recently-formed convective layer is composed of many convective cells, with horizontal size approximately the height of the layer. As the layer increases its thickness by incorporating fluid from below, both the aspect ratio of the flow and the number of convective cells within the layer decrease. Once the aspect ratio of the growing convective layer reaches a critical size, convective plumes become vertically-sheared by a large scale horizontal flow. We find the critical aspect ratios between 1.2 – 1.7, being smaller at $Pr = 0.1$ (Fig. 1a).

In this problem convection is driven by the temperature difference across the thermal boundary layer due to the imposed heat flux at the top, and the convective layer grows in time. This means that the Rayleigh number Ra grows in time and its magnitude is set by the thickness of the convective layer.

We find that once the zonal flow sets in, the convective layer stops growing and Ra saturates to a roughly constant value, $Ra \sim 10^8$, 5×10^8 , 10^9 , and 5×10^9 for $Pr = 7$, 1, 0.5, and 0.1, respectively. To illustrate this behaviour, Fig. 1(b) shows the temporal evolution of Ra for the cases using $F_0/F_{\text{crit}} = 10.8$.

The stalling of the convective layer growth is explained by the reduced vertical transport of sheared convective plumes. In a normal situation absent of strong horizontal flows, kinetic energy in the convective plumes or eddies is used to lift and mix fluid from below, increasing the convection zone thickness [20, 23]. However, in the situation considered here, the zonal flow disperses the convective plumes and takes energy from them. As a result, the flow near the convective boundary does not have enough energy to lift and mix fluid from below, thereby the convection zone does not grow. The latter can be inferred from the horizontally-averaged flux profiles considering just the contribution from convective motions, which in our dimensionless form is given by $\bar{F}_H^{\text{conv}} = \bar{w}T$, where $\bar{\cdot}$ denotes the average over the horizontal direction. We observe in Fig. 2 that after the zonal flow arises ($t \geq 0.01 t_{\text{diff}}$), the convective heat flux near the interface decreases. Further, the position of the interface slightly changes with time, meaning that the rate at which the outer convection zone grows becomes smaller. We note how the zonal flow affects the shape of the convective flux profiles at $t = 0.012 t_{\text{diff}}$, changing from being roughly linear within the outer convection zone (the expected profile not affected by the zonal flow) to a profile with roughly two different cooling rates (smaller near the bottom of the layer).

Figure 3 shows profiles of the x -component of the flow velocity normalized to its maximum magnitude, $\bar{u}/\max|\bar{u}|$. The profiles are computed after the zonal flow appears. As expected, since the boundaries do not impose stress on the flow, we find the maximum of the flow at the top boundary. The horizontal flow at the bottom of the convective layer, which is oppositely directed to the flow at the top, reaches about 0.4-0.5 of the maximum flow velocity, suggesting that there must be transport of momentum across the convective boundary. We do not find any trend regarding the direction of the zonal flow, in some of the simulations positive (negative) momentum is transported upward (downward), and vice-versa. However, we find for all the cases that once the zonal flow sets in, its direction is never reversed during the simulation.

The onset of the zonal flow can be observed in the time series of the horizontal and vertical rms velocities, $\langle u^2 \rangle^{1/2}$ and $\langle w^2 \rangle^{1/2}$, respectively, where $\langle \cdot \rangle$ denotes the average over the entire domain. As an example, we show in Fig. 4 the temporal evolution of $\langle u^2 \rangle^{1/2}$ and $\langle w^2 \rangle^{1/2}$, for all cases using $F_0/F_{\text{crit}} = 5.4$. We observe that during the early evolution, both rms velocities increase with time having roughly the same magnitude. This is expected since in this stage the convection zone grows and the fluid flow is dominated by cellular motions. However, once the instability that triggers the zonal flow arises, there is a large increase in $\langle u^2 \rangle^{1/2}$, and a substantial decrease in $\langle w^2 \rangle^{1/2}$, meaning that a significant fraction of the work done by buoyancy forces is transformed to kinetic energy but enhancing mainly the horizontal fluid motions. Note that for $Pr \leq 1$, the time series of the rms veloci-

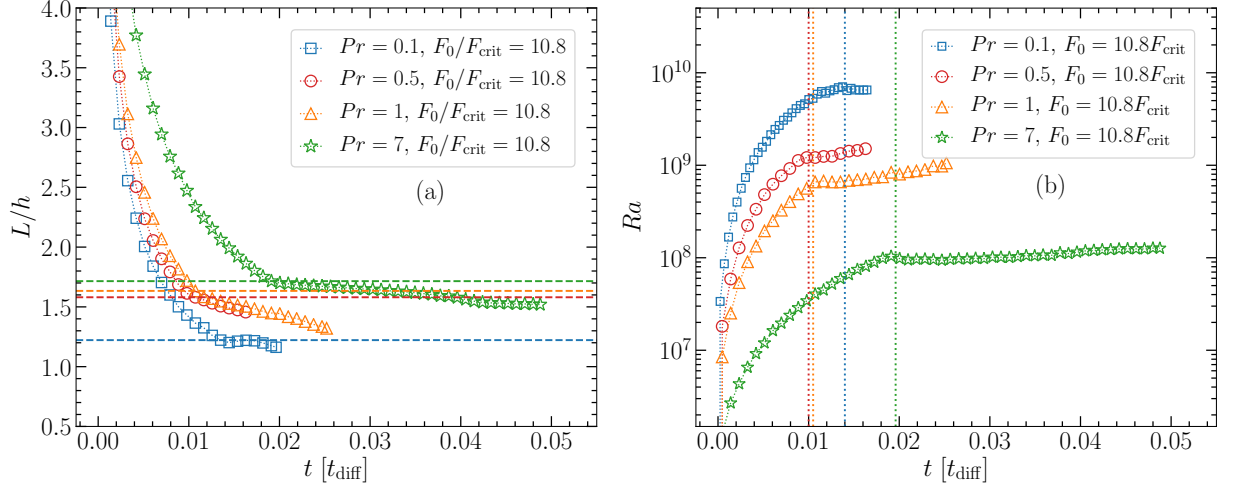


FIG. 1. Panel (a): Ratio between the width of the domain, L , and the thickness of the convective layer, h (i.e., the aspect ratio of the flow within the convective layer) as a function of time. The dashed horizontal lines denote the value of the aspect ratio when the zonal flow sets in. Panel (b): Rayleigh number as a function of time. Once the zonal flow sets in (vertical lines), the magnitude of Ra varies slowly with time (flat region). In both panels, the results are shown for simulations at $F_0/F_{\text{crit}} = 10.8$. Colors and symbols distinguish between simulations at different Pr , as shown in the legends. The rest of the simulations behave in a similar way but on different time scales and magnitudes.

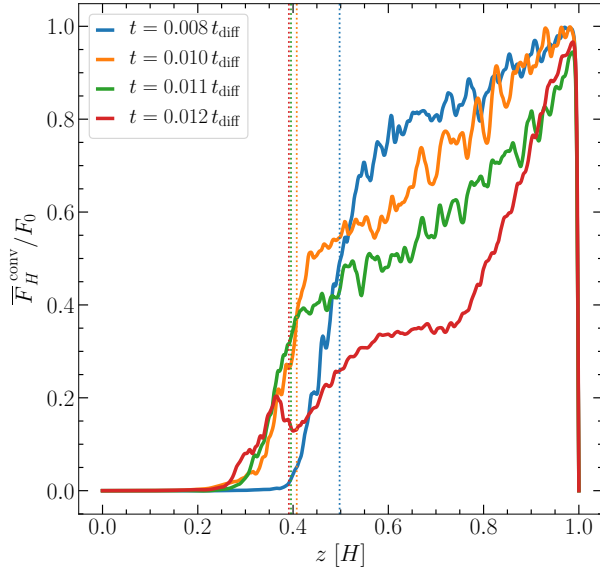


FIG. 2. Horizontally-averaged profiles of the convective flux divided by the imposed heat flux, $\overline{F}_H^{\text{conv}} / F_0$. Results are shown at different times for the case at $Pr = 1$, $F_0/F_{\text{crit}} = 10.8$. The vertical lines set the position of the convective boundary at the times when profiles are shown. Colors distinguish between different times. We recall that for this case, from $t \geq 0.01 t_{\text{diff}}$ the fluid is affected by the zonal flow.

ties exhibit oscillations or bumps, whereas for $Pr = 7$ it does not. The difference in the behaviour of the rms velocities distinguish between the bursting and non-bursting regime of the system.

The bursting and non-bursting regimes have substantial differences in the vertical transport. These differences are more clear when we look into the time series of the heat flux aver-

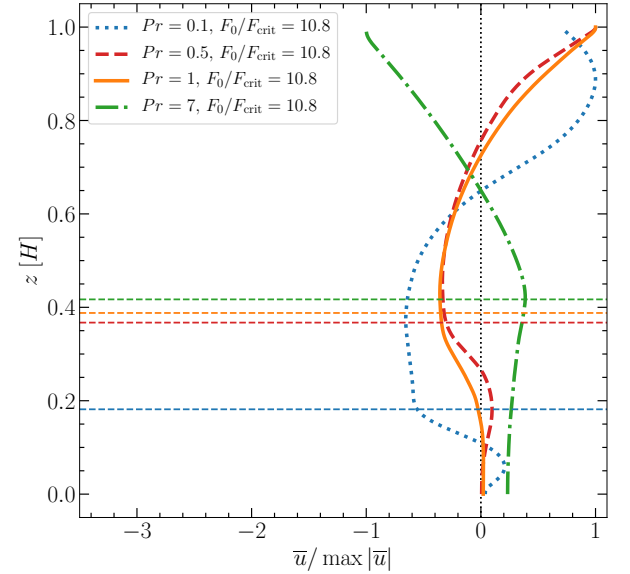


FIG. 3. Vertical profiles of the horizontal flow velocity, \overline{u} , normalized to its maximum magnitude, $\max |\overline{u}|$. Colors and line-styles distinguish between different Pr . All the cases correspond to simulations using $F_0/F_{\text{crit}} = 10.8$. The horizontal lines denote the position of the convective boundary. Note that for $Pr = 7$, there is also contribution from the advection of secondary convective layers in the fluid (see Figs. 7c and 8c-d), and therefore the horizontal flow velocity does not decay to zero towards the bottom of the box.

aged over the whole domain, which in dimensionless form is given by

$$\langle F_H \rangle = \langle wT \rangle - \langle dT/dz \rangle, \quad (13)$$

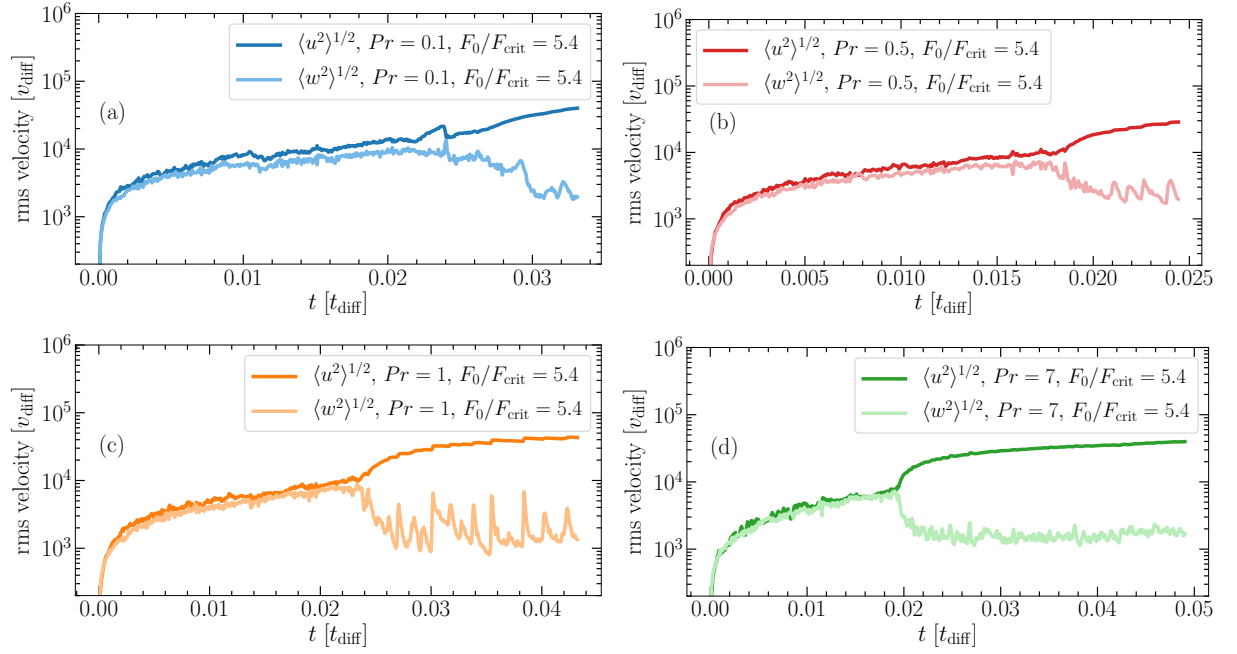


FIG. 4. Panels (a)-(d): Temporal evolution of the horizontal and vertical rms velocity (dark and light colors) for different Pr using $F_0/F_{\text{crit}} = 5.4$. Note that panels do not share the same scale in the time axis. The time series for the cases using $F_0/F_{\text{crit}} = 10.8$ are similar but the instability appears earlier and the magnitude of $\langle u^2 \rangle^{1/2}$ is higher.

where the first and second terms correspond to the convective and diffusive heat flux, respectively.

Figure 5 shows time series of the ratio $\langle F_H \rangle / F_0$ for all our simulations. We observe for all the cases that as the convection zone grows, the convective contribution to the heat flux increases with time and dominates the magnitude of $\langle F_H \rangle / F_0$. Once the zonal flow arises and is strong enough to disperse convective plumes and reduce the vertical kinetic energy, $\langle F_H \rangle / F_0$ decays. The subsequent evolution of the heat flux is different depending on Pr . For the cases $Pr \leq 1$, the vertical transport occurs through discrete bursts whose intensity and frequency increase with Pr . Each burst is separated by a quiescent phase in which $\langle F_H \rangle / F_0 \approx 15 - 20\%$ of its value before the onset of the zonal flow.

Figure 6 shows the different stages of a burst. In the quiescent phase (a), convective plumes are constantly dispersed by the zonal flow. This flow suppresses convective instabilities until it has decayed sufficiently for convective plumes to appear again (b) and the fluid suddenly overturns (c). The fluid is energized by buoyancy and circulation motions, but once again, kinetic energy is transferred to the zonal flow, convective plumes get dispersed, and a new quiescent phase begins (d).

Note that although $\langle F_H \rangle / F_0$ decays during the quiescent phase, its value is not negligible since the averaged heat flux across the box is more than 10% of the imposed heat flux in all the cases. The reason for this can be explained using the flux profiles during the quiescent phase (see Fig. 7a). We observe that near the top boundary there are still convective motions that contribute to heat transport. This is expected since the fluid surrounding the top boundary is constantly cooling down

by the imposed flux, thereby it has a permanent energy source to undergo convection. We also observe a smaller contribution to heat transport due to convective motions at the bottom of the outer convective layer ($z \approx 0.4$) and below it due to secondary convective layers at $z \approx 0.25$ (Fig. 8a-b). We recall that the flux time series in Fig. 5 take into account the flux averaged over the whole box, however, even if we just consider the average over the outer convective layer, $\langle F_H \rangle / F_0$ would be still non-negligible. On the contrary, during the bursting phase as soon as the zonal flow weakens, the much colder fluid at the top sinks catastrophically in the way of a Rayleigh-Taylor plume, increasing significantly the heat flux (Fig. 7b).

Finally, the cases $Pr = 7$ are different, we do not observe bursts and rather than cellular motions, convective plumes vertically sheared dominate the flow within the convective layer. In those cases, the contribution of the convective flux to the total flux is significant at all times (Fig. 7c). Further, as for the cases $Pr \leq 1$, the diffusive and convective flux profiles in Fig. 7c (and also the snapshots in Fig. 8a-b) show that secondary convective layers form in the fluid, being responsible of the subsequent increase in $\langle F_H \rangle / F_0$.

Since this work is focused on zonal flows and their properties, an analysis of layer formation and its evolution is going to be presented in a future paper. However, it is worth mentioning that the zonal flow is able to destabilize the convective boundary to Kelvin-Helmholtz instabilities (clearly seen in Fig. 8c), causing strong mixing and eventually forming secondary convective layers [this mechanism is known as thermohaline shear instability, see, e.g., 24, 25].

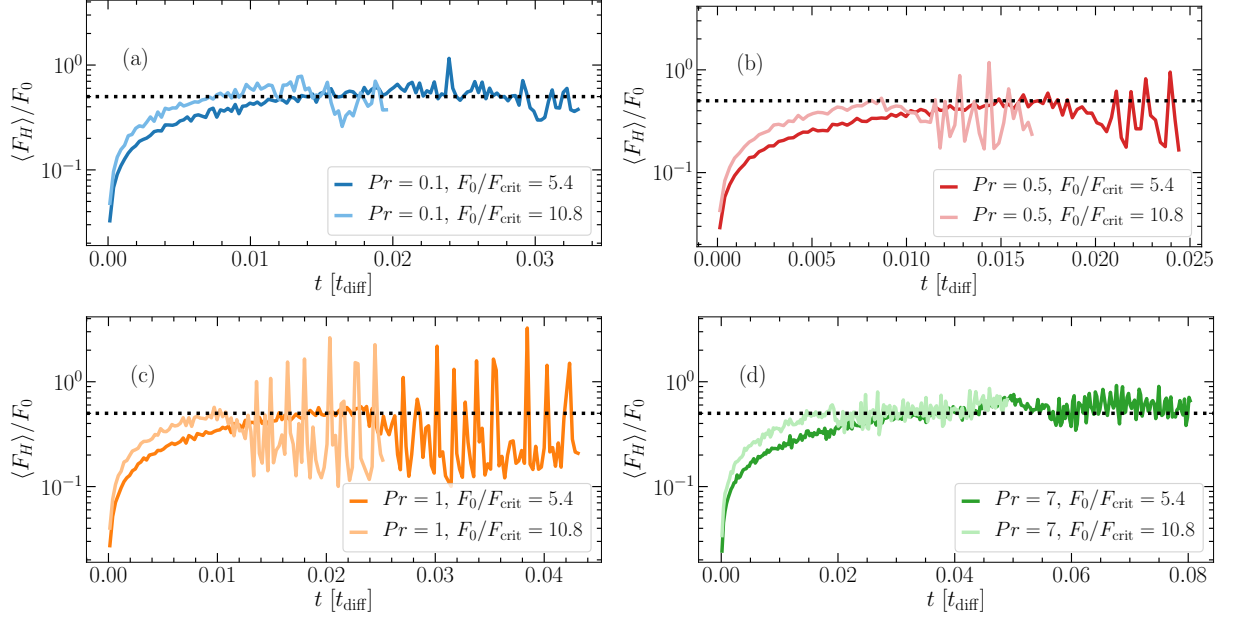


FIG. 5. Time series of the averaged heat flux (divided by the imposed flux at the top), $\langle F_H \rangle / F_0$ for $Pr = 0.1, 0.5, 1$, and 7 (panels a, b, c, and d, respectively). Colors distinguish between $F_0/F_{\text{crit}} = 5.4$ (dark) and $F_0/F_{\text{crit}} = 10.8$ (light). Note that panels do not share the same scale in the time axis. In all panels the dashed lines corresponds to $\langle F_H \rangle / F_0 = 0.5$, i.e., the expected averaged ratio if the whole fluid cools at a constant rate.

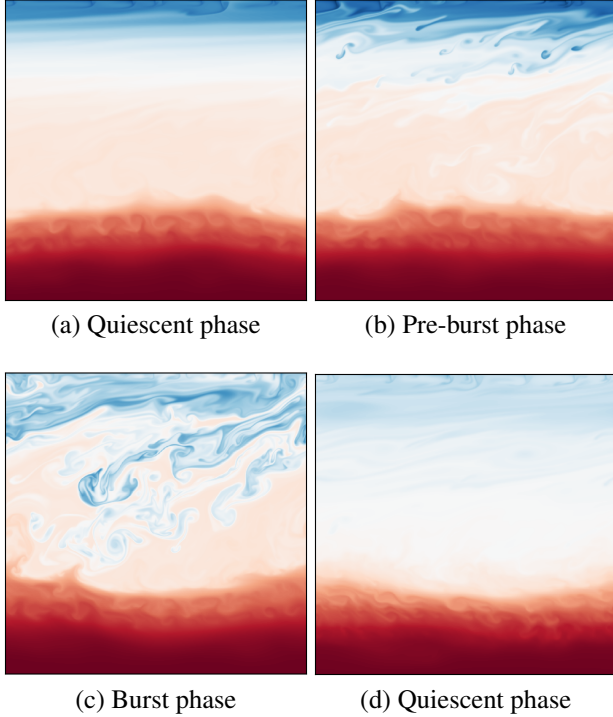


FIG. 6. Instantaneous snapshots of the temperature field during a single burst, for the case $Pr = 1, F_0/F_{\text{crit}} = 10.8$. Blue and red colors represent cold and hot fluid, respectively. The color scale is not the same in all panels.

B. Suppression of zonal flows in wider domains

We have shown that for square domain simulations (i.e., $L/H = 1$), the zonal flow always appears when the aspect ratio of the convective layer, L/h , is smaller than approximately two (Fig. 1a). For illustrative purposes, we show in Fig. 9(a) the effect of increasing the width of the domain on the evolution of the rms velocities for the case $Pr = 1, F_0/F_{\text{crit}} = 5.4$. We find that for $L/H \geq 2$, both the horizontal and vertical rms velocities increase gradually in time, without the instabilities observed for $L = H$. Further, the curves lie on top of each other no matter the value of L . Fig. 9(b) shows the effect of increasing the width of the domain on the time series of the averaged heat transport. We find that the bursting regime disappears at large aspect ratio and the system evolves toward a state in which the whole fluid cools at a constant rate with $\langle F_H \rangle / F_0 \approx 0.5$. We perform additional simulations for $Pr = 0.1, 1$, and 7 and find the same behaviour. During the whole evolution of the simulations, the growing convective layer has an aspect ratio that is always much larger than two and thereby zonal flows are not expected to arise.

The suppression of the zonal flow has important consequences on the evolution of the flow. First, the vertical transport is always significant and never through quasi-periodic bursts. Second, the spatial structure of the flow is different. Whereas the square domain simulations have flows dominated by sheared convective plumes and bursts, the wider domain simulations exhibit convective cells which persist in time. Third, the convective layer never stops growing and reaches the bottom of the box mixing the whole fluid.

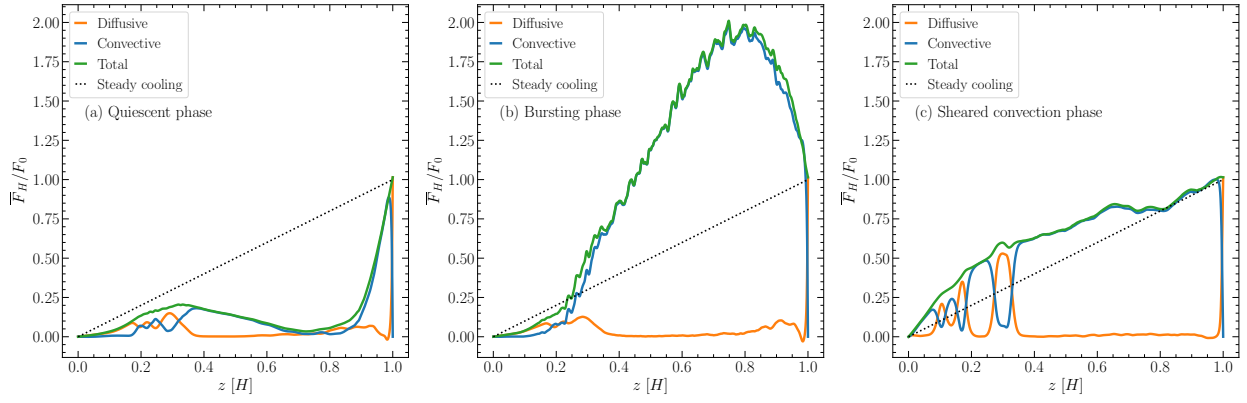


FIG. 7. Horizontally-averaged profiles of the ratio between the heat flux and the imposed flux, \bar{F}_H/F_0 . Panel (a) shows the profiles during the quiescent phase, whereas Panel (b) shows the profiles for a particular burst during the active phases. Both panels show results for a typical burst in the simulation $Pr = 1$, $F_0/F_{\text{crit}} = 10.8$. Panel (c) shows the profiles during the sheared convection phase observed in all simulations at $Pr = 7$. The results are shown for the case $Pr = 7$, $F_0/F_{\text{crit}} = 5.4$ at $t = 0.065$. In all panels, the green, blue, and orange lines correspond to the total, advective, and diffusive contribution to the flux, respectively. The dotted line corresponds to the expected profile if the whole fluid cools down at a constant rate, i.e., $\bar{F}_H/F_0 = z$.

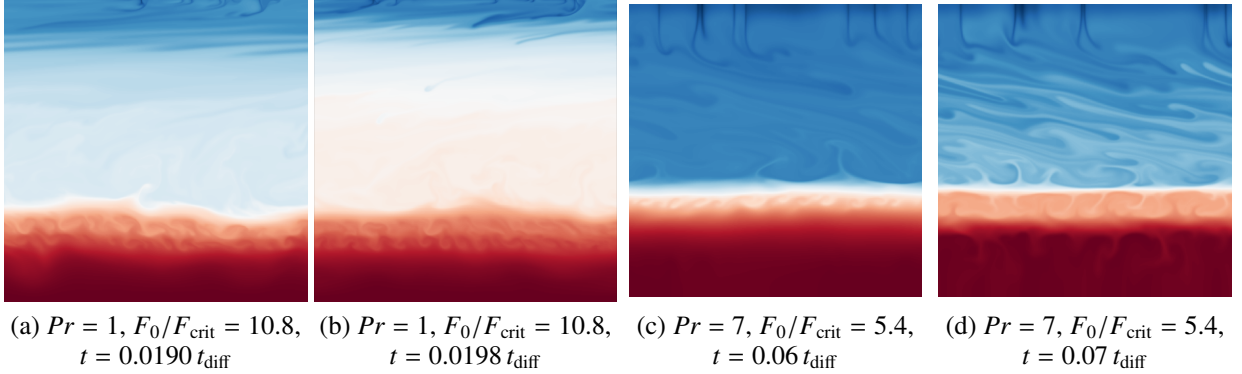


FIG. 8. Instantaneous snapshots of the temperature field for the cases $Pr = 1$, $F_0/F_{\text{crit}} = 10.8$ (panels a and b), and $Pr = 7$, $F_0/F_{\text{crit}} = 5.4$ (panels c and d). Blue and red colors represent cold and hot fluid, respectively. The color scale is not the same for all panels. The times were chosen to show that secondary layers form and contribute to the averaged heat transport (in the quiescent phase for the case of panels a and b, and during the non-bursting regime for the case of panels c and d).

IV. SUMMARY AND DISCUSSION

We studied the onset and evolution of zonal flows when a convective layer propagates into a fluid with a stable composition gradient. We considered different values of the Prandtl number, $Pr = 0.1, 0.5, 1$, and 7 . Our goal was to provide a novel way to study zonal flows and shear effects since the growing convective layer allows exploration of a wide range of values of the Rayleigh number and aspect ratios. Our results confirm and extend to convection with stable composition gradients at low Pr previous findings in experiments of thermal and fingering convection.

In summary:

1. In square domain simulations ($L/H = 1$), zonal flows and their shear effects always arise as long as the aspect ratio of the convective layer is smaller than approximately two. The critical aspect ratio for the onset zonal

flows seems to depend on Pr , being smaller at low Pr (Fig 1a).

2. Once the zonal flow sets in, convective plumes get dispersed by the flow and the convective layer stops growing. The stalling of the convection zone results in a saturation of the Rayleigh number toward a constant value in time, $Ra \sim 10^8 - 5 \times 10^9$, where the smallest and largest values correspond to the cases using $Pr = 7$, and 0.1 , respectively (Fig. 1b).
3. As found in previous numerical simulations of pure thermal convection, the morphology and evolution of the flow depends on the Prandtl number. On the one hand, for $Pr \leq 1$ the flow organizes into discrete bursts in which convective plumes suddenly overturn quasi-periodically, with smaller transport between bursts (Figs. 5a-c, 6, and 7a). On the other hand, for $Pr = 7$ the flow consists of sheared convective plumes

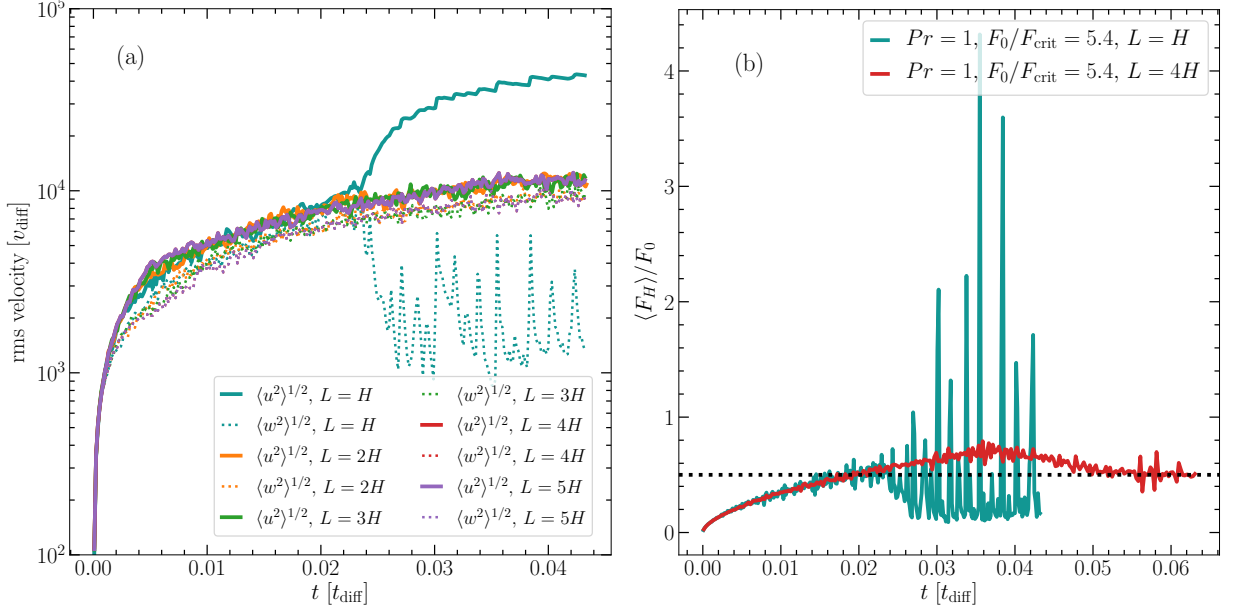


FIG. 9. Panel (a): Temporal evolution of the horizontal and vertical rms velocities ($\langle u^2 \rangle^{1/2}$ and $\langle w^2 \rangle^{1/2}$, using solid and dotted lines, respectively), for different domain width L (using different colors). Panel (b): Time series of the averaged heat flux divided by the imposed flux at the top ($\langle F_H \rangle / F_0$), for simulations using different domain widths ($L = H$ and $L = 4H$, as shown in the legends). In both panels, the results correspond to experiments with $Pr = 1$, $F_0/F_{\text{crit}} = 5.4$.

instead of bursts, and the convective transport is sustained at all times (Figs. 5d and 7c).

4. The bursting regime is stronger at $Pr = 1$ and weakens for $Pr < 1$ (Fig. 7).
5. We observe the formation of secondary convective layers in all the simulations considered in this work (Fig. 8). The new layers contribute to the averaged heat transport at all times for both the non-bursting and bursting regimes (Fig 7).
6. For wider domains ($L/H \geq 2$), the aspect ratio of the convective layer is always much larger than two and zonal flows never develop during the evolution of the simulations (Figs. 9a-b). The absence of large scale horizontal flow means that the the growth of the convective layer is uninterrupted, and the fluid fully mixes in all the cases considered.

We have shown that zonal flows also arise in the time-dependent problem of a convective layer propagating into a stable fluid. Our work differs from previous studies by considering a stable composition gradient and the fact that convection is driven by a constant heat flux at the top boundary rather than a constant temperature contrast across the fluid depth.

We find the onset of the zonal flow when the aspect ratio of the convection zone is smaller than two and $Ra \sim 10^8 - 10^{10}$. The values of Ra are narrower than in previous work. For example, Goluskin *et al.* [6] found zonal flows can arise when $Ra \sim 10^4 - 10^{10}$. A possible explanation could be the fact that in our problem convection occurs just in a portion of the fluid

domain and the bottom of the convection zone is not stress-free, meaning that horizontal fluid motions at the bottom of the layer are decreased due to the interaction with the motionless (stable) fluid below. On the contrary, in Goluskin *et al.* [6] convection occurs in the whole box, and the stress-free boundaries enhance at all times the horizontal fluid motions, which is favourable for instabilities that give rise to the zonal flow.

Despite the differences mentioned above, the zonal flow and its effects are similar to those reported in previous work. In particular, the transition from the bursting to the non-bursting regime seems to occur at $Pr \simeq 1$ no matter how convection is driven in the system of whether the fluid has composition gradients. We did not explore in detail the range of Pr in which the system reaches the bursting regime. However, we find the intensity and frequency of the bursts to decrease for $Pr < 1$.

Recent work by Wang *et al.* [19] explored in detail the influence of the aspect ratio of the domain on the evolution of the zonal flow in thermal convection. By imposing initial conditions consistent with a linear shear-flow, and pure convective rolls, Wang *et al.* [19] found that the zonal flow only persists or arises when the aspect ratio of the domain is smaller than a certain value depending on Ra and Pr . For larger values, simulations initialized with convective cells do not develop sheared-flows, and the ones initialized with zonal flows experiment a transition to convective cells. Those results support previous findings by Fitzgerald and Farrell [5], who demonstrated that in fluid domains of large aspect ratio, the tilting instability that enhances zonal flows can be suppressed due to the non-linear interaction of horizontal modes of the ve-

locity field. We did not perform a spectral analysis to reveal the physical mechanism behind the zonal flow, but our simulations including composition gradients seem to exhibit the same behaviour. We find that zonal flows only appear when the aspect ratio of the convective zone is smaller than two, and that it can be suppressed using wider fluid domains (see Figs. 1 and 9).

The zonal flow and its effects are a problem for two-dimensional studies of convective transport and mixing in fluids where strong shear flows are not expected to appear. For example, layer formation and transport across diffusive interfaces in double-diffusive convection [7, 19]. However, the fact that zonal flows do not appear at large aspect ratio suggests that two-dimensional simulations could still be useful to study convection and related problems involving stable composition gradients (such as convective overshoot). We did not explore different boundary conditions, however, additional

simulations with the numerical set-up of Garaud and Brummell [7] but using a much larger aspect ratio would be of great interest in order to see if zonal flows can also be avoided in that situation.

ACKNOWLEDGMENTS

This work was supported by an NSERC Discovery Grant. J.R.F. acknowledges support from a McGill Space Institute (MSI) Fellowship. A. C. and J. R. F. are members of the Centre de Recherche en Astrophysique du Québec (CRAQ) and the Institut de recherche sur les exoplanètes (iREx). This research was enabled in part by support provided by Calcul Québec (calculquebec.ca), and Compute Canada (www.computeCanada.ca). Computations were performed on Graham and Béluga.

-
- [1] M. Evonuk and G. A. Glatzmaier, 2D Studies of Various Approximations Used for Modeling Convection in Giant Planets, *Geophysical and Astrophysical Fluid Dynamics* **98**, 241 (2004).
 - [2] M. Heimpel and J. Aurnou, Turbulent convection in rapidly rotating spherical shells: A model for equatorial and high latitude jets on Jupiter and Saturn, *Icarus* **187**, 540 (2007).
 - [3] J. M. Finn, Nonlinear interaction of Rayleigh-Taylor and shear instabilities, *Physics of Fluids B* **5**, 415 (1993).
 - [4] E. P. van der Poel, R. Ostilla-Mónico, R. Verzicco, and D. Lohse, Effect of velocity boundary conditions on the heat transfer and flow topology in two-dimensional rayleigh-bénard convection, *Phys. Rev. E* **90**, 013017 (2014).
 - [5] J. G. Fitzgerald and B. F. Farrell, Mechanisms of mean flow formation and suppression in two-dimensional Rayleigh-Bénard convection, *Phys. Fluids* **26**, 054104 (2014).
 - [6] D. Goluskin, H. Johnston, G. R. Flierl, and E. A. Spiegel, Convectively driven shear and decreased heat flux, *J. Fluid Mech.* **759**, 360–385 (2014).
 - [7] P. Garaud and N. Brummell, 2D or Not 2D: The Effect of Dimensionality on the Dynamics of Fingering Convection at Low Prandtl Number, *Astrophys. J.* **815**, 42 (2015).
 - [8] J.-H. Xie, K. Julien, and E. Knobloch, Jet formation in salt-finger convection: a modified Rayleigh-Bénard problem, *J. Fluid Mech.* **858**, 228 (2019).
 - [9] P. Garaud, A. Kumar, and J. Sridhar, The Interaction between Shear and Fingering (Thermohaline) Convection, *Astrophys. J.* **879**, 60 (2019).
 - [10] R. Thompson, Venus’s General Circulation is a Merry-Go-Round., *Journal of Atmospheric Sciences* **27**, 1107 (1970).
 - [11] N. H. Bian and O. E. Garcia, Confinement and dynamical regulation in two-dimensional convective turbulence, *Physics of Plasmas* **10**, 4696 (2003).
 - [12] L. N. Howard and R. Krishnamurti, Large-scale flow in turbulent convection: a mathematical model, *J. Fluid Mech.* **170**, 385 (1986).
 - [13] W. V. R. Malkus, Discrete Transitions in Turbulent Convection, *Proceedings of the Royal Society of London Series A* **225**, 185 (1954).
 - [14] R. Krishnamurti and L. N. Howard, Large-scale flow generation in turbulent convection, *Proceedings of the National Academy of Sciences* **78**, 1981 (1981).
 - [15] T. Hartlep, A. Tilgner, and F. H. Busse, Large scale structures in rayleigh-bénard convection at high rayleigh numbers, *Phys. Rev. Lett.* **91**, 064501 (2003).
 - [16] E. H. Anders and B. P. Brown, Convective heat transport in stratified atmospheres at low and high Mach number, *Phys. Rev. Fluids* **2**, 083501 (2017).
 - [17] J. M. Massaguer, E. A. Spiegel, and J. P. Zahn, Convection-induced shears for general planforms, *Phys. Fluids* **4**, 1333 (1992).
 - [18] P. C. Matthews, A. M. Rucklidge, N. O. Weiss, and M. R. E. Proctor, The three-dimensional development of the shearing instability of convection, *Phys. Fluids* **8**, 1350 (1996).
 - [19] Q. Wang, K. L. Chong, R. J. A. M. Stevens, R. Verzicco, and D. Lohse, From zonal flow to convection rolls in Rayleigh-Bénard convection with free-slip plates, arXiv e-prints , arXiv:2005.02084 (2020), [arXiv:2005.02084 \[physics.flu-dyn\]](https://arxiv.org/abs/2005.02084).
 - [20] J. R. Fuentes and A. Cumming, Penetration of a cooling convective layer into a stably-stratified composition gradient: entrainment at low Prandtl number, arXiv e-prints (2020).
 - [21] E. A. Spiegel and G. Veronis, On the Boussinesq Approximation for a Compressible Fluid., *Astrophys. J.* **131**, 442 (1960).
 - [22] K. J. Burns, G. M. Vasil, J. S. Oishi, D. Lecoanet, and B. P. Brown, Dedalus: A flexible framework for numerical simulations with spectral methods, *Phys. Rev. Research* **2**, 023068 (2020).
 - [23] M. J. Molemaker and H. A. Dijkstra, The formation and evolution of a diffusive interface, *J. Fluid Mech.* **331**, 199–229 (1997).
 - [24] T. Radko, Thermohaline layering in dynamically and diffusively stable shear flows, *J. Fluid Mech.* **805**, 147–170 (2016).
 - [25] P. Garaud, The formation of diffusive staircases, *J. Fluid Mech.* **812**, 1–4 (2017).